European Journal of Radiology 192 (2025) 112403

Contents lists available at ScienceDirect

European Journal of Radiology

journal homepage: www.elsevier.com/locate/ejrad

Accelerating non-contrast MR angiography of the thoracic aorta using compressed SENSE with deep learning reconstruction

Jan P. Janssen [a,*], Roman J. Gertz [a], Juliana Tristram [a], Marvin A. Spurek [a], Kenan Kaya [a], Robert Terzis [a], Robert Hahnfeldt [a], Thorsten Gietzen [b], David Maintz [a], Thorsten Persigehl [a], Kilian Weiss [c], Lenhard Pennig [a], Carsten Gietzen [a]

[a] Institute for Diagnostic and Interventional Radiology, Faculty of Medicine and University Hospital Cologne, University of Cologne, Cologne, Germany
[b] Department of Cardiology, Heart Center, Faculty of Medicine and University Hospital Cologne, University of Cologne, Cologne, Germany
[c] Philips Healthcare Germany, Hamburg, Germany

A R T I C L E I N F O

Keywords:
Thoracic aorta
Magnetic resonance angiography
Non-contrast-enhanced magnetic resonance angiography
Compressed sensing
Deep Learning

A B S T R A C T

Purpose: REACT (Relaxation-Enhanced Angiography without ContrasT) is a reliable non-contrast magnetic resonance angiography for imaging of the thoracic aorta but remains time-consuming. This study evaluates acceleration of image acquisition using compressed sensing and parallel imaging (Compressed SENSE, CS) combined with deep learning-based image reconstruction (CS-AI).
Methods: In this prospective single-center study, 40 volunteers underwent ECG- and navigator-triggered 3D REACT at 3 T using CS acceleration factor 4 (CS4; reference standard) and 8 (CS8). CS8 data were reconstructed with standard and CS-AI methods (CS8-AI). Two radiologists measured aortic diameters, rated subjective image quality and performed pairwise comparisons. Additionally, objective image quality metrics were calculated.
Results: Median scan time was reduced by 44 % (CS4: 8:41 min; CS8/CS8-AI: 4:52 min). All techniques showed excellent agreement in aortic diameter measurements (mean differences < 0.2 mm; $P > 0.999$). CS8-AI demonstrated reduced mean absolute deviation from CS4 compared to CS8 (0.67 vs. 0.77 mm; $P = 0.003$), and measurement variance was 40–50 % lower with CS8-AI than with CS8 (inter-/intrarater: $P < 0.001$), and comparable to CS4. CS8 showed significantly lower subjective image quality scores than CS4 (3.70[3.33–4.00] vs. 4.25[3.90–4.50]; $P < 0.001$), while CS8-AI showed comparable or higher scores (4.40[4.00–4.70]; $P = 0.076$). Forced-choice comparisons favored CS4 over CS8 (90 % vs. 2.5 %; $P < 0.001$), but no preference was observed between CS4 and CS8-AI (42.5 % vs. 37.5 %; $P > 0.999$). Objective metrics predominantly confirmed the subjective results.
Conclusion: Deep learning-based reconstruction enables the acquisition of REACT of the thoracic aorta in less than five minutes while preserving high image quality and maintaining excellent measurement reproducibility.

1. Introduction

Diseases of the thoracic aorta, including aneurysms, dissection, and stenosis are often asymptomatic for a long time and only recognized when acute, life-threatening complications arise [1]. Early diagnosis and regular follow-up are crucial for risk stratification and treatment planning, especially in high-risk populations with connective tissue disorders like Marfan or Loeys-Dietz syndrome [2].

Magnetic resonance angiography (MRA) is well-established for monitoring abnormal findings and risk groups, as it does not involve ionizing radiation. Non-contrast MRA techniques offer several benefits: they avoid contrast-related side effects or mistiming of a contrast bolus,

Abbreviations: 2D, Two-dimensional; 3D, Three-dimensional; aCNR, Apparent contrast-to-noise ratio; aSNR, Apparent signal-to-noise ratio; bSSFP, balanced steady-state free precession; CI, 95% confidence interval; CS, Compressed SENSE; CS-AI, Compressed SENSE with adaptive intelligence reconstruction; CTA, Computed tomography angiography; ECG, Electrocardiogram; ERD, Edge-rise distance; ICC, Intraclass correlation coefficients; IQR, Interquartile range; LoA, 95% limits of agreement; MRA, Magnetic resonance angiography; MRI, Magnetic resonance imaging; REACT, Relaxation-Enhanced Angiography without ContrasT; SD, Standard deviation; SENSE, Sensitivity Encoding; τ, Kendall's tau.

* Corresponding author at: Institute for Diagnostic and Interventional Radiology, University Hospital Cologne, Kerpener Str. 62, Cologne 50937, Germany.
E-mail address: jan.janssen@uk-koeln.de (J.P. Janssen).

https://doi.org/10.1016/j.ejrad.2025.112403
Received 23 July 2025; Received in revised form 25 August 2025; Accepted 1 September 2025
Available online 2 September 2025

Table 1
Volunteer characteristics.

Age (mean ± SD)	58.13 ± 5.03 years	
Height (mean ± SD)	1.74 ± 0.11 m	
Weight (mean ± SD)	79.85 ± 17.74 kg	
BMI (mean ± SD)	26.40 ± 5.83 kg/m^2	
	n	**%**
Gender		
Female	23	57.5 %
Male	17	42.5 %
Cardiovascular risk factors		
Hypertension	12	30.0 %
Diabetes mellitus	3	7.5 %
Smoking	9	22.5 %
Coronary artery disease	1	2.5 %

BMI = Body mass index.

Table 2
Scan parameters.

Scan	CS4	CS8	CS8-AI
CS acceleration factor	4	8	8
Reconstruction	standard	standard	AI
Nominal scan time	4:48 min	2:24 min	2:24 min
K-space trajectory	Cartesian		
Acquisition orientation	Coronal		
Acquired voxel size	1.5 x 1.5 x 1.5 mm^3		
Reconstructed voxel size	0.67 x 0.67 x 0.75 mm^3		
Field of view (FH x RL x AP)	300 x 375 x 150 mm^3		
T2 preparation	50 ms		
Repetition time	4.6 ms		
Echo times	1.38 / 2.8 ms		
Flip angle	12°		

AP = anterior posterior; CS4 = Compressed SENSE acceleration factor 4; CS8 = CS acceleration factor 8; CS8-AI = CS8 with Adaptive-CS-Net reconstruction; FH = feet head; REACT = Relaxation-Enhanced Angiography without ContrasT; RL = right left.

streamline workflows and reduce costs, and allow repeated imaging if examinations are non-diagnostic [3,4]. Furthermore, ECG and respiratory synchronization are routinely employed for non-contrast MRA techniques, while contrast enhanced-MRA is generally acquired without synchronization, leading to increased motion artifacts [5]. Nevertheless, currently established techniques, especially at high spatial resolution, often require long acquisition times of up to twelve minutes, depending on magnetic field strength, acquisition parameters, navigator efficiency, and acceleration strategy, which limits their use in clinical routine [5–9]. 2D and 3D balanced steady-state free precession (bSSFP) are widely used for non-contrast aortic MRA due to their high signal-to-noise ratio and excellent blood-background contrast [4]. However, they are highly sensitive to B_0 inhomogeneities, causing banding artifacts, especially with metallic implants, pulsatile flow or at higher magnetic field strengths [10]. Relaxation-Enhanced Angiography without ContrasT (REACT) offers improved robustness to B_0 inhomogeneities by combining magnetization preparation with a 3D Dixon-based water-fat separated readout [11,12] enabling robust isotropic non-contrast and flow-independent MRA over a wide field of view and has shown excellent performance in imaging of the supra-aortic arteries [13–15], pulmonary vasculature [16], congenital heart disease [17,18] and thoracic aorta [3,8,19,20]. Although these techniques already achieve relatively short acquisition times through acceleration methods such as parallel imaging, compressed sensing, and their combination, they still require more time than the widely used contrast-enhanced MRA [3,19], and acceleration is limited by an increase in image noise and a decrease in image quality when using high acceleration factors [21,22].

To address these limitations, Pezzotti et al. [23,24] introduced a deep learning-based reconstruction technique called Adaptive-CS-Net (CS-AI) in 2019. CS-AI integrates both parallel imaging and compressed sensing with a convolutional neural network, which enhances data sparsity within an unrolled iterative reconstruction framework. This leads to improved noise suppression and enables higher acceleration factors whiles preserving detail. Previous studies have already demonstrated significant reductions in acquisition time for cardiac cine bSSFP [25], non-contrast MRA of the coronary arteries [26], and cervical REACT [27]. Therefore, the aim of this study was to assess whether CS-AI enables further acceleration of thoracic REACT while preserving image quality and the reproducibility of aortic measurements.

2. Materials and methods

2.1. Study design and population

This prospective single-center study was approved by our institutional review board on March 23, 2022 (reference number: 20-1296_1) and registered in the German Clinical Trials Register on September 15, 2022 (reference number: DRKS00030210).

Recruitment of 41 volunteers and data acquisition took place between November 2023 and June 2024. Written informed consent was obtained from all participants. The inclusion criterion was an age of over 18 years and the absence of general contraindications for MRI. Participants with incomplete scan data were excluded. Prior to image acquisition, the age, height, weight, gender and cardiovascular risk factors were recorded (Table 1).

2.2. MRI

3D thoracal REACT was acquired in coronal orientation at a 3 T MRI system (Philips MR 7700; *Philips Healthcare, Best, The Netherlands*) with a 28-channel coil for cardiac imaging.

A 50 ms T2 preparation and an inversion recovery pulse with a two-point DIXON readout (mDIXON XD; *Philips Healthcare, Best, The Netherlands*) were used [3]. To account for cardiac and respiratory motion, ECG-triggering (end-diastolic) and a diaphragmatic navigator were implemented. An 8 mm gating window was selected to ensure adequate navigator efficiency within the ECG-triggered framework at 3 T; narrower windows (5–7 mm) were considered but risked prolonged and variable scan times in free-breathing volunteers.

The k-space acquisition scheme was based on a variable density incoherent undersampling pattern with a more densely sampled k-space center [28]. Two acquisitions were conducted using the same acquisition and post-processing pipeline: REACT accelerated with a combination of parallel imaging and compressed sensing (Compressed SENSE; CS [28]) acceleration factor 4 (CS4; nominal scan time 4:48 min, representing the current clinical standard employed at our institution) and REACT with CS acceleration factor 8 (CS8; nominal scan time 2:24 min). The order of acquisition was switched after one half of the volunteers had been scanned to mitigate any ordering or learning bias. Table 2 shows additional scan parameters.

2.3. MRI reconstruction

All image reconstructions were performed using standard hardware and software as provided by the manufacturer of the MRI system with reconstruction times of about 25 s (CS; Compressed SENSE, *Philips Healthcare, Best, The Netherlands*) and 50 s (CS-AI; SmartSpeed, *Philips Healthcare, Best, The Netherlands*), respectively. Reconstruction time was measured in a representative as the interval from data acquisition completion to image availability. Both reconstruction methods were applied to the same 8-fold undersampled raw k-space data (CS8/CS8-AI), whereas 4-fold undersampled datasets were reconstructed using CS only (CS4). CS-AI embeds a convolutional neural network within an unrolled iterative framework, preserving physical priors (coil sensitivities, k-space consistency) [23,24]. It was trained on a large MR dataset of various anatomical regions (~740,000 images at 1.5 T/3 T). More details regarding the reconstruction algorithms can be found in the supplementary data.

2.4. Image analysis

Image analysis was performed using a commercially available image viewer (DeepUnity Diagnost, release 1.1.1.1; *Dedalus HealthCare GmbH, Bonn, Germany*). Source images and maximum intensity projections with optional window levelling and angulation were assessed. Two radiologists (3 and 8 years of experience in cardiovascular MRI; hereafter R1 and R2) evaluated the randomized images, blinded to patient data, acquisition and reconstruction protocol. To minimize potential recall bias, image sets were evaluated in separate sessions with a minimum interval of four weeks between assessments of the same subject in different reconstruction variants.

2.5. Aortic diameter measurements

Aortic diameter measurements (inner edge to inner edge approach [29]) were performed at the following five levels: aortic annulus, aortic sinus, sinotubular junction (STJ), ascending aorta (at the level of the pulmonary trunk), and at the descending aorta (30 mm distal of the left subclavian artery). The measurements were taken in two orthogonal axes (maximum and its perpendicular diameter) at each level; only in the aortic sinus three measurements were taken (cusp-to-cusp). R1 repeated all measurements after an additional four-week interval to determine intrarater agreement.

2.6. Subjective image quality

The same aortic levels were subjectively evaluated on a 5-point Likert scale (1 = non-diagnostic; 5 = excellent) regarding overall image quality, noise, aortic edge sharpness, and artifacts. Detailed definitions of the scoring criteria are provided in Supplementary Table S1.

For pairwise forced-choice comparison, two images of each subject were presented side by side to the blinded readers who had to choose which image they preferred for ruling out vascular pathologies (CS4 vs CS8, CS4 vs CS8-AI, CS8 vs CS8-AI).

Vascular findings. Furthermore, R1 and R2 assessed MRA datasets for the presence of vascular findings such as anatomical variants or pathologies. In this context, Ectasia was defined as segmental dilatation exceeding age-, sex-, and body surface area-adjusted norms; aneurysm as $\geq$ 1.5 times the expected diameter. Reference values were based on Kawel-Boehm et al. [30].

Fat-water swapping artifacts. Water maps of REACT were evaluated by R1 for the presence of fat–water swapping artifacts as well as the corresponding signal of the in-phase image at the respective signal loss of the water map, if present [14,15,31].

2.7. Objective image quality

A radiologist in training with four years of experience in cardiovascular MRI (R3) assessed objective image quality parameters: Apparent signal-to-noise ratio (aSNR), apparent contrast-to-noise ratio (aCNR) and aortic Edge-rise distance (ERD). Details on the methods are provided in the supplementary data.

2.8. Statistical analysis

Statistical analysis was performed using R (v4.3.1) and GraphPad Prism (v10.4.2, GraphPad Software, Boston, MA, USA). Categorical variables are reported as counts and percentages; continuous and ordinal variables as mean ± standard deviation, or median (interquartile range), as appropriate. Normality was assessed using the Shapiro-Wilk test and Q-Q plots.

Methods were compared using mean differences, absolute differences, and 95 % limits of agreement (LoA). Agreement was quantified by intraclass correlation coefficients (ICC; two-way mixed-effects, absolute agreement) with 95 % confidence intervals and variance, and compared using Fisher's z-transformation and F-tests.

Interreader agreement was assessed using Kendall's tau (τ). ICC and τ were interpreted as: slight (0.01–0.2), fair (0.21–0.4), moderate (0.41–0.6), substantial (0.61–0.8), and almost perfect (0.81–1.0).

Subjective and objective parameters were compared using paired t-tests or Wilcoxon signed-rank tests. Forced-choice responses were pooled and analyzed with binomial tests.

$P < 0.05$ (two-sided) was considered statistically significant. Bonferroni correction was applied for multiple comparisons; exploratory subanalyses were not adjusted.

Table 3
Aortic diameters per level and differences in measurements.

Level	CS4	CS8	CS8-AI
Annulus [mm]	25.06 ± 2.98	25.28 ± 3.02	25.20 ± 2.91
Sinus [mm]	35.69 ± 4.78	35.62 ± 4.73	35.82 ± 4.73
STJ [mm]	30.67 ± 3.84	30.55 ± 3.78	30.86 ± 3.88
Ascending [mm]	33.68 ± 4.24	33.68 ± 4.40	33.70 ± 4.28
Descending [mm]	24.94 ± 2.76	25.00 ± 2.80	25.02 ± 2.76
Differences in measurements compared to CS4			
Mean absolute diff. [mm]	–	**0.77 ± 0.68***	**0.67 ± 0.61***
Mean diff. [mm]	–	0.087 ± 1.03	0.085 ± 0.90
95 %-LoA [mm]	–	(−1.93–2.10)	(−1.67–1.84)

*Significant difference between CS8 and CS8-AI in absolute deviation from CS4 ($P = 0.003$; paired *t*-test); CS4 = Compressed SENSE acceleration factor 4; CS8 = Compressed SENSE acceleration factor 8; CS8-AI = Compressed SENSE acceleration factor 8 with adaptive intelligence reconstruction; diff. = difference; LoA = limits of agreement; STJ = sinotubular junction

3. Results

3.1. Study population and baseline characteristics

Forty-one volunteers received REACT of the thoracic aorta using CS4 and CS8. One participant had to be excluded due to incomplete scan data. Consequently, 40 subjects were included (epidemiological data and cardiovascular risk factors are provided in Table 1).

3.2. Scan duration

While the nominal scan time was preset to 4:48 min (CS4) and 2:24 min (CS8/CS8-AI), the median total acquisition time was reduced by 44 % from 8:41 min [8:31–8:57] for CS4 to 4:52 min [4:47–4:58] for CS8/CS8-AI ($P < 0.001$).

3.3. Aortic diameter measurements

Aortic diameters obtained with CS4, CS8, and CS8-AI showed close agreement across all five predefined anatomical levels, with mean differences of less than 0.2 mm between sequences (Table 3). Mean absolute differences to CS4 were lower for CS8-AI (0.67 ± 0.61 mm) than for CS8 (0.77 ± 0.68 mm; $P = 0.003$). Bland-Altman analysis revealed narrow LoA for all comparisons, with the smallest range observed between CS8 and CS8-AI. LoAs relative to CS4 were consistently narrower in CS8-AI than in CS8 (Fig. 1A).

In the interrater and intrarater analysis, all sequences demonstrated excellent agreement. CS8-AI achieved the highest ICC, the smallest mean difference, and the lowest variance. The variance was significantly lower compared to CS8, but not significantly different from CS4.

Bland-Altman plots for inter- and intrarater reproducibility are shown in Fig. 1B and 1C; detailed reproducibility metrics are provided in Table 4.

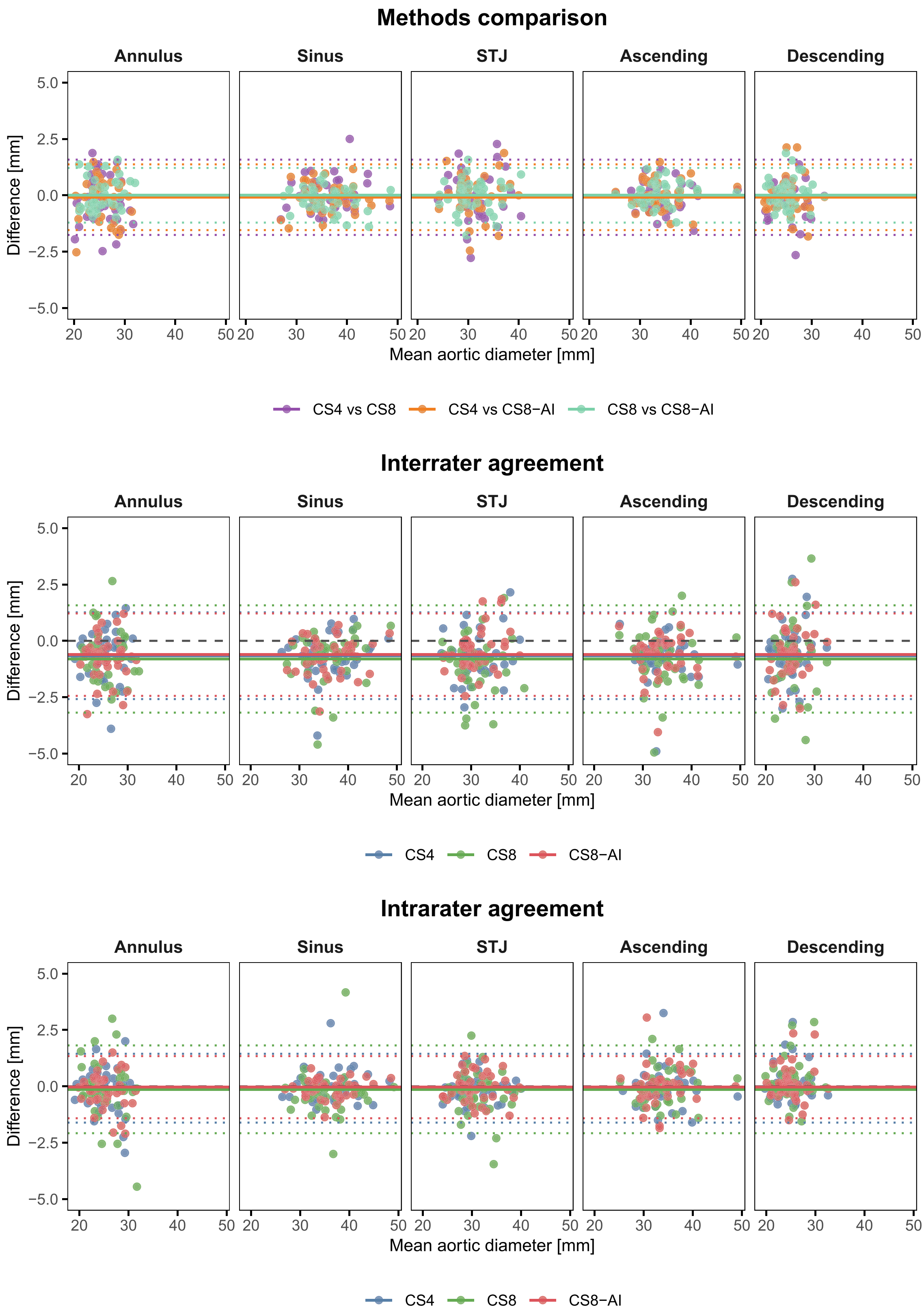

Fig. 1. Bland-Altman plots depicting the agreement between the respective methods (CS4, CS8, CS8-AI; A) as well as the reproducibility within a method between two readers (B) and with repeated measurement of one reader (C). Each row contains one plot per measurement level with three data sets. The colored lines show the mean difference and the dotted lines the 95 % limits of agreement, each averaged over all measurement levels (aortic annulus, aortic sinus, STJ, ascending aorta, and at the descending aorta) for better comparability. CS4 = Compressed SENSE acceleration factor 4; CS8 = Compressed SENSE acceleration factor 8; CS8-AI = Compressed SENSE acceleration factor 8 with adaptive intelligence reconstruction; STJ = sinotubular junction.

Table 4
Inter- and intrarater reproducibility of aortic diameter measurements.

Parameter	CS4	CS8	CS8-AI	CS4 vs CS8	CS4 vs CS8-AI	CS8 vs CS8-AI
Interrater agreement						
ICC (95 %-CI)*	0.986 (0.981 to 0.989)	0.978 (0.97 to 0.983)	0.987 (0.983 to 0.99)	z = 2.21 (P = 0.081)†	z = − 0.44 (P > 0.999)†	**z = − 2.65 (P = 0.024)†**
Mean diff. [mm]	−0.66 ± 0.98	−0.81 ± 1.21	−0.61 ± 0.93	–	–	–
95 %-LoA [mm]	(−2.58–1.26)	(−3.18–1.57)	(−2.44–1.22)	–	–	–
Variance (mm^2)	0.96	1.47	0.87	**F = 0.65 (P = 0.008)‡**	F = 1.11 (P > 0.999)‡	**F = 1.69 (P < 0.001)‡**
Intrarater agreement						
ICC (95 %-CI)*	0.991 (0.988 to 0.993)	0.985 (0.981 to 0.989)	0.993 (0.99 to 0.994)	**z = 2.42 (P = 0.046)†**	z = − 0.99 (P = 0.97)†	**z = − 3.41 (P = 0.002)†**
Mean diff. [mm]	−0.082 ± 0.78	−0.13 ± 0.99	−0.037 ± 0.70	–	–	–
95 %-LoA [mm]	(−1.61–1.44)	(−2.08–1.82)	(−1.42–1.34)	–	–	–
Variance [mm^2]	0.61	0.99	0.49	**F = 0.61 (P = 0.002)‡**	F = 1.23 (P = 0.45)‡	**F = 1.99 (P < 0.001)‡**

*All ICC values: P < 0.001; † Fisher-z-test (ICC comparison); ‡ F-test of measurement variance (n = 200 pairs, df = 199, 199); CS4 = Compressed SENSE acceleration factor 4; CS8 = Compressed SENSE acceleration factor 8; CS8-AI = Compressed SENSE acceleration factor 8 with adaptive intelligence reconstruction; diff. = difference; ICC = intraclass correlation coefficients (two-way mixed-effects model, absolute agreement); LoA = limits of agreement.

Table 5
Subjective image quality scores.

	CS4 median [IQR]	CS8 median [IQR]	CS4 vs CS8 (P; Wilcoxon)	CS8-AI median [IQR]	CS4 vs CS8-AI (P; Wilcoxon)	Kendall's tau (τ)*
Image Quality (Overall)	4.25 [3.90–4.50]	3.70 [3.33–4.00]	**< 0.001**	4.40 [4.00–4.70]	0.076	0.80
Annulus	3.50 [3.00–4.00]	3.00 [2.50–3.50]	**< 0.001**	4.00 [3.00–4.00]	0.24	0.73
Sinus	4.00 [3.13–4.00]	3.50 [3.00–4.00]	**0.003**	4.00 [3.50–5.00]	**0.029**	0.78
STJ	4.00 [4.00–4.88]	3.75 [3.00–4.00]	**< 0.001**	4.00 [4.00–5.00]	0.55	0.74
Ascending	4.75 [4.00–5.00]	4.00 [4.00–4.00]	**< 0.001**	5.00 [4.50–5.00]	0.25	0.78
Descending	5.00 [5.00–5.00]	4.25 [4.00–5.00]	**< 0.001**	5.00 [5.00–5.00]	>0.999	0.72
Noise	4.20 [3.82–4.48]	3.40 [2.83–3.70]	**< 0.001**	4.50 [4.10–4.80]	**< 0.001**	0.82
Edge	4.20 [3.65–4.48]	3.85 [3.33–4.10]	**< 0.001**	4.25 [3.83–4.58]	0.87	0.75
Artifacts	4.35 [3.90–4.60]	3.90 [3.45–4.28]	**< 0.001**	4.50 [4.00–4.70]	0.15	0.76

*All τ values: P < 0.001; CS4 = Compressed SENSE acceleration factor 4; CS8 = Compressed SENSE acceleration factor 8; CS8-AI = Compressed SENSE acceleration factor 8 with adaptive intelligence reconstruction.

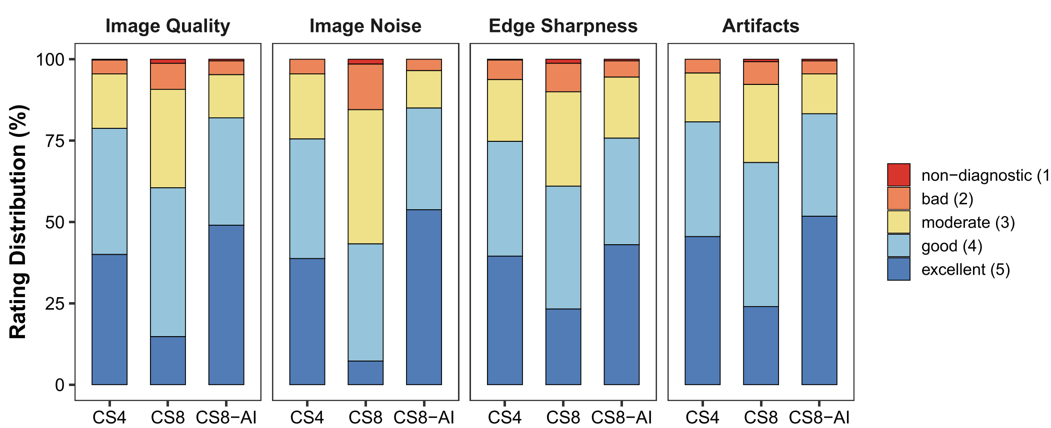

Fig. 2. Cumulative distribution of subjective scores for Compressed SENSE acceleration factor 4 (CS4) and acceleration factor 8 with (CS8-AI) and without (CS8) adaptive intelligence reconstruction in the categories image quality, image noise, edge sharpness and artifacts using a 5-point Likert scale.

3.4. Subjective image quality

CS8-AI achieved subjective image quality, edge sharpness and artifact ratings comparable to the standard reference CS4, while CS8 was rated consistently lower across all evaluated parameters (Table 5). Perceived image noise was rated significantly higher in CS8 than in CS4, whereas CS8-AI showed even less impairing noise than CS4. Inter-reader agreement was substantial across all subjective parameters. Distributions of subjective ratings are illustrated in Fig. 2.

Pairwise forced-choice comparisons confirmed the superiority of CS8-AI over CS8 and the equivalence of CS8-AI and CS4. Readers significantly favored CS4 over CS8 (P < 0.001) and CS8-AI over CS8 (P < 0.001), with no preference between CS8-AI and CS4 (P > 0.999). Detailed results are shown in Supplementary Table S2.

Representative image examples of CS4, CS8 and CS8-AI are shown in Figs. 3–6.

3.5. Vascular findings

One aneurysm (2.5 % [1 of 40]; Fig. 4) of the thoracic aorta, some ectasias (25 % [10 of 40]; e.g. Fig. 5), common origins of the carotid arteries (12.5 % [5 of 40]) and an aberrant subclavian artery (2.5 % [1 of 40]; Fig. 5) were found equally in CS4, CS8, and CS8-AI by both readers. No further vascular findings were reported.

3.6. Fat-water swapping artifacts

Fat-water swapping artifacts were observed in 7 volunteers (17.5 %),

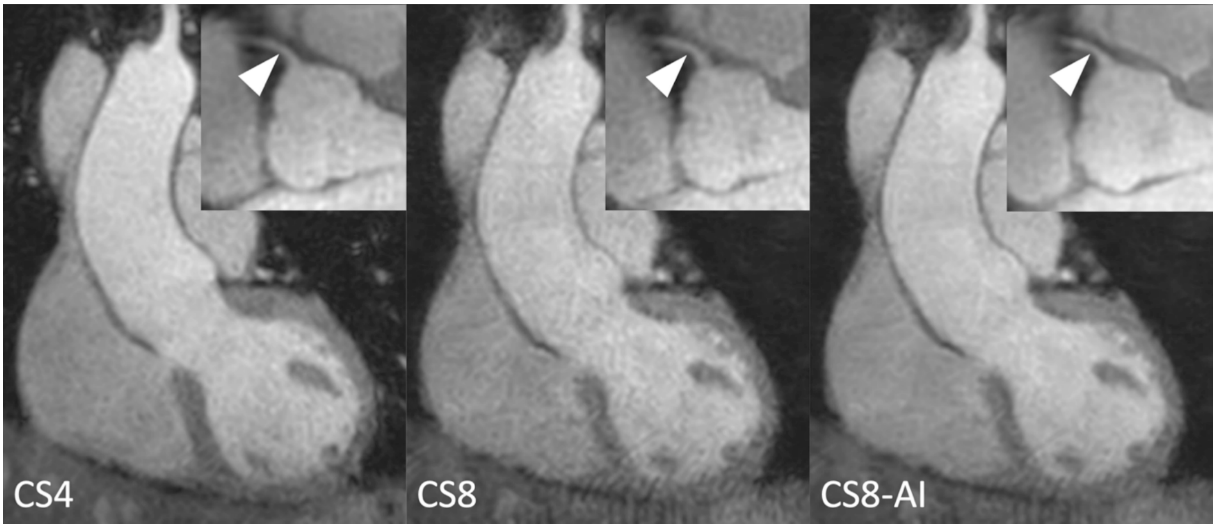

Fig. 3. Example of a healthy 58-year-old male volunteer. Coronal source images of the three methods (the reference standard Compressed SENSE acceleration factor 4 (CS4) and acceleration factor 8 with (CS8-AI) and without (CS8) adaptive intelligence reconstruction) with axial inserts at the level of the origin of the right coronary artery (arrowhead). CS8 shows a higher image noise and poorer delineation of the right coronary artery compared to CS4, which could be significantly improved in CS8-AI.

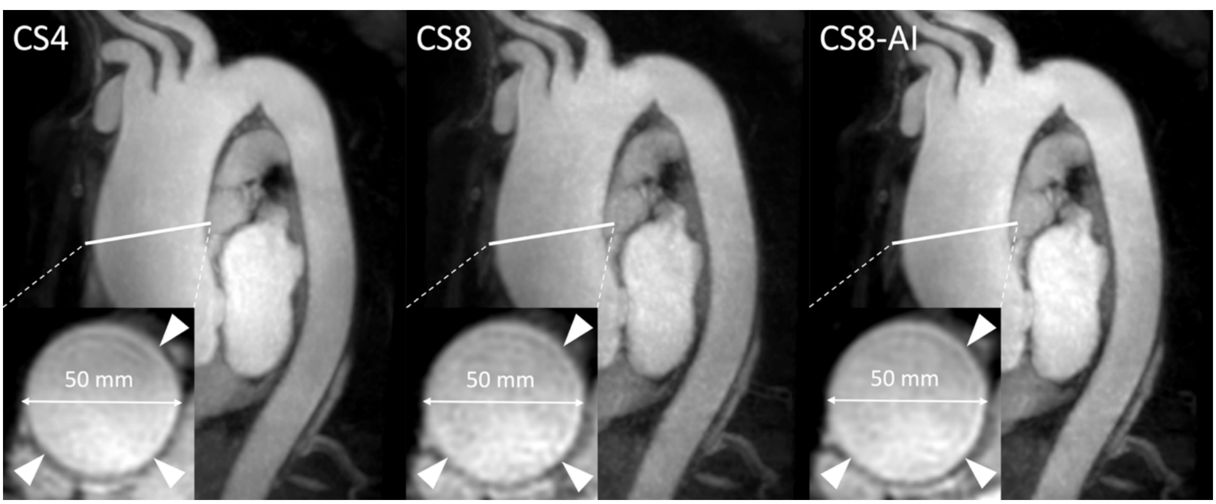

Fig. 4. Incidental finding of a long fusiform aneurysm of the ascending aorta (maximum diameter 50 mm) in a 57-year-old female volunteer without known cardiovascular risk factors. Images of methods (the reference standard Compressed SENSE acceleration factor 4 (CS4) and acceleration factor 8 with (CS8-AI) and without (CS8) adaptive intelligence reconstruction) are shown as parasagittal reformation (maximum intensity projection, 10 mm slice thickness) with inserts of reformations perpendicular to the aortic lumen at the level of the maximum diameter (0.67 mm slice thickness). The inserts illustrate the differences in image noise. While CS8 has a more impairing noise than CS4, this difference could be diminished using CS8-AI. This example suggests that the delineation of the aortic edge (arrowheads) may also suffer from interfering noise and may lead to a less precise or less reproducible measurements.

most frequently affecting the left subclavian artery (n = 6), and in one case also the adjacent common carotid artery. One artifact was located in the right hepatic vein. In one subject, the artifact appeared only in CS8 and CS8-AI but not in CS4; in another, it was present in CS4 and CS8 but absent in CS8-AI. All artifacts were clearly distinguishable as such by a focal signal drop in the water-only map and a corresponding signal increase in the fat-only map.

3.7. Objective image quality

Overall, CS8 achieved lower aSNR and aCNR than CS4 while CS8-AI yielded similar aSNR and aCNR compared to CS4 (Supplementary Table S3). There were no significant differences regarding the ERD of the ascending aorta compared to CS4 (Supplementary Table S4). Corresponding plots are shown in Fig. 7.

4. Discussion

This study evaluated the potential of CS-AI to accelerate non-contrast MRA of the thoracic aorta using REACT. The main findings demonstrate that CS-AI enables a 44 % reduction in scan time compared to the current clinical standard without impairment of subjective and objective measures of image quality, while preserving reproducibility of aortic diameter measurements.

There was no significant difference in aortic diameter measurements between methods, mean differences to the clinical reference (CS4) remained below 0.2 mm, and limits of agreement were narrow without evidence of systematic bias. These small deviations are in line with prior reproducibility studies, where inter-method mean differences typically ranged from 0.3–1 mm with limits of agreement up to ± 2–3 mm and interreader ICCs consistently > 0.95 [4,5,8,10,20,29]. In fact, they are

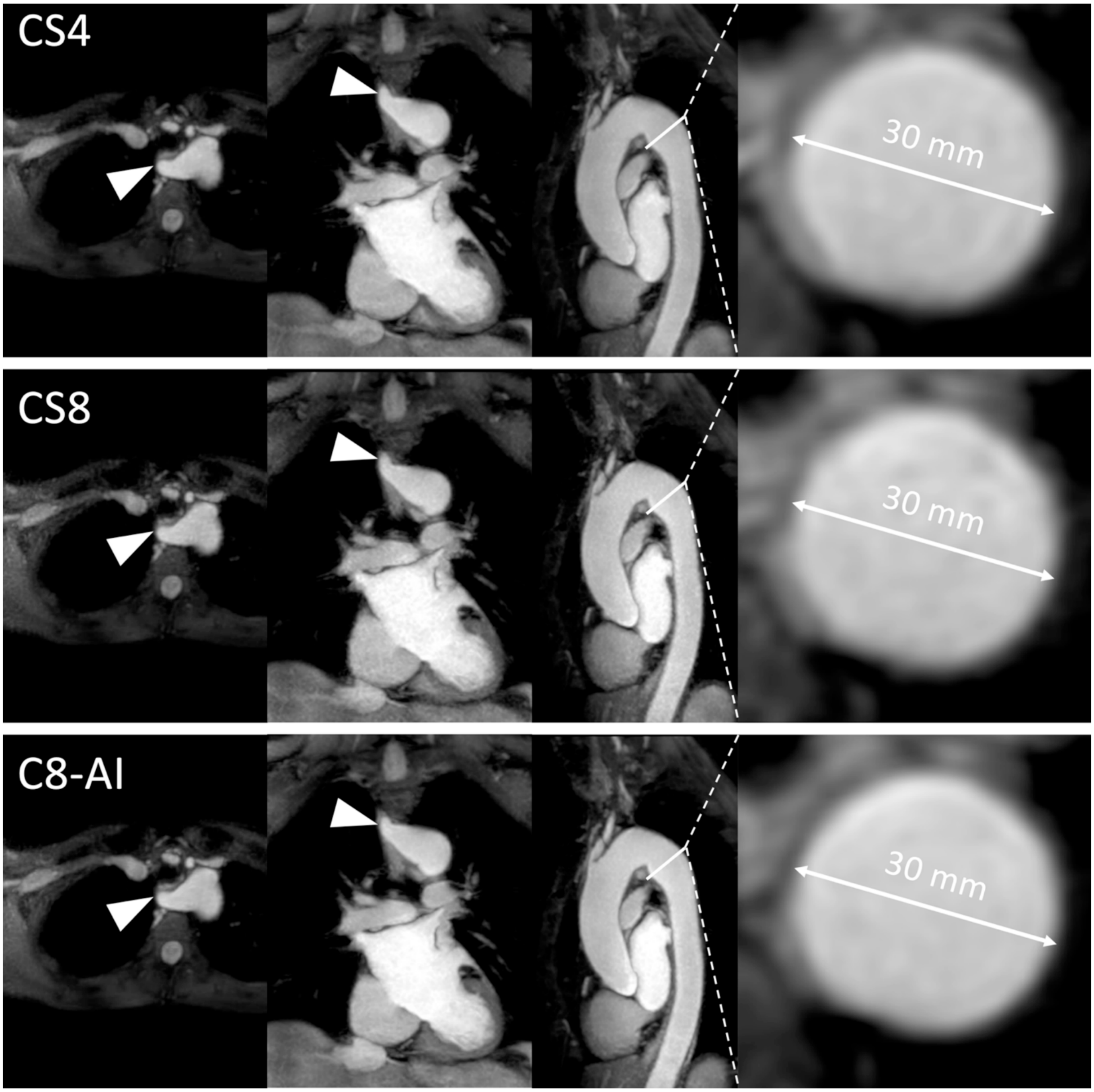

Fig. 5. Incidental finding of an aberrant subclavian artery (arrowheads) and a focal ectasia of the proximal descending aorta in a 64-year-old female volunteer. Axial, coronal and parasagittal views (maximum intensity projections, 5 mm slice thickness) of the reference standard Compressed SENSE acceleration factor 4 (CS4) and acceleration factor 8 with (CS8-AI) and without (CS8) adaptive intelligence reconstruction. Right images show magnified reformations perpendicular to the aortic lumen corresponding to the white line in the parasagittal view (0.67 mm slice thickness). Compared to CS4, CS8 offers lower image quality with higher noise, while CS8-AI clearly mitigates these limitations.

smaller than those reported by Wright et al. for 3D Dixon versus 2D SSFP in Marfan patients [8], and comparable to values observed by Veldhoen et al. and von Knobelsdorff-Brenkenhoff et al. in comparisons of non-contrast and contrast-enhanced MRA [4,5]. CS8-AI yielded the lowest variance and highest ICCs, albeit all methods provided excellent results. Moreover, interreader variability in this study exceeded the differences between methods, indicating that measurement precision is predominantly reader-driven. Nevertheless, the magnitude of interreader differences in this study remained within the range described in the literature [32]. Such reliability is particularly desirable in clinical follow-up examinations, for instance in Marfan patients, where average annual progression rates range between 0.03 mm (abdominal aorta) and 0.24 mm (aortic sinus) or even up to 0.77 mm (proximal descending aorta) after aortic root replacement [33]. The high reproducibility of CS8-AI may be explained by a stabilizing effect of deep learning-based reconstruction, which reduces noise and thus inter-reader variability in high-resolution accelerated datasets [23,25,27]. This is particularly relevant for subtle or borderline findings. The lower variance between CS8 and CS8-AI than between either technique and CS4 can be explained by the use of identical raw data for both reconstructions, while CS4 was recorded separately. The most pronounced discrepancy was observed in the proximal descending aorta, likely due to varying interpretations of its location relative to the left subclavian artery and the presence of focal ectasia near the isthmus. These findings emphasize the need for standardized measurement protocols in longitudinal imaging [32].

Regarding image quality, highly accelerated compressed sensing alone (CS8) was associated with inferior subjective and objective results, whereas the addition of CS-AI effectively mitigated these limitations. Notably, subjective image quality and vessel sharpness with CS8-AI were comparable to CS4, and noise perception was even lower. This indicates that CS-AI reconstruction not only recovers degraded signal but improves visual impression in accelerated protocols. While a previous

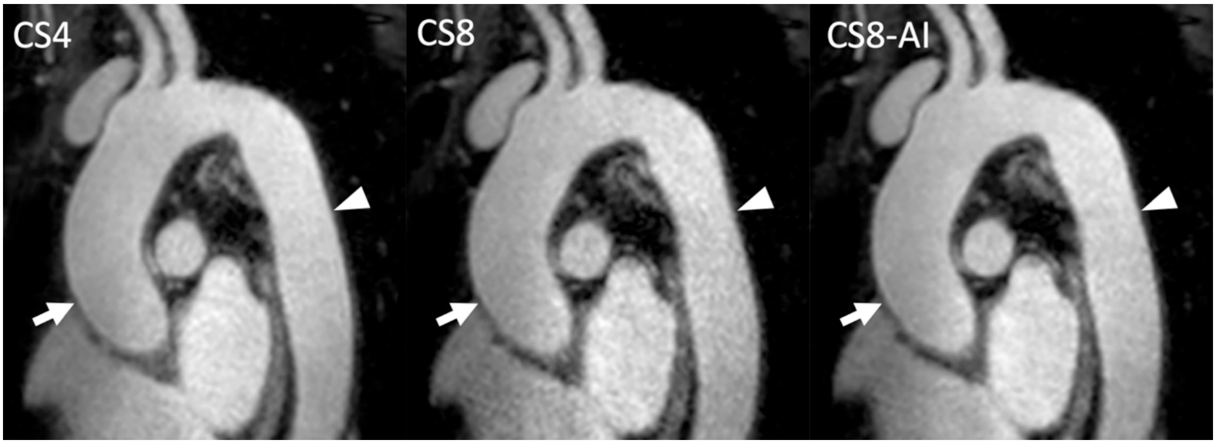

Fig. 6. Thoracic aorta of a healthy 50-year-old male volunteer in parasagittal view (slice thickness 0.67 mm). Compared to the reference standard (Compressed SENSE acceleration factor 4, CS4), imaging with an acceleration factor of 8 (CS8) provides reduced image quality and increased noise, impairing the delineation of the aortic edges (exemplary area marked by an arrow for the ascending aorta and an arrowhead for the descending aorta). In contrast, CS8 with adaptive intelligent reconstruction (CS8-AI) restores image quality to a level comparable to CS4.

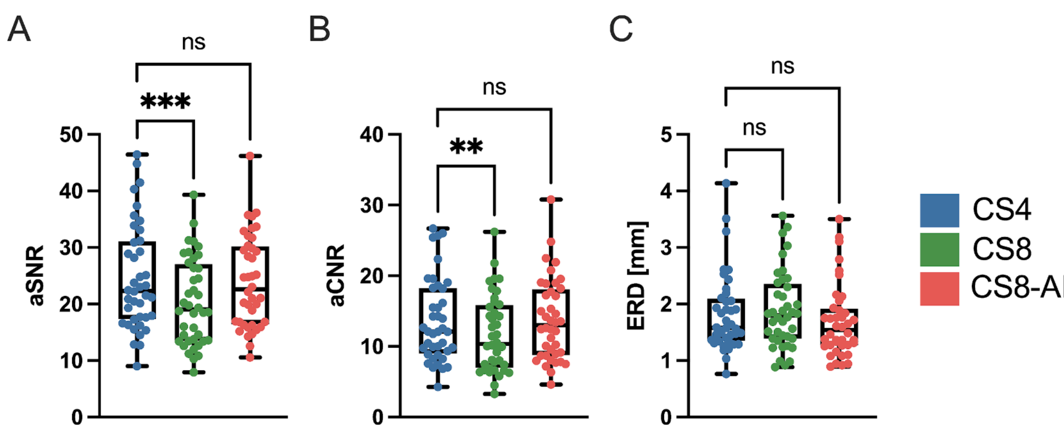

Fig. 7. Scatter plots with box-and-whisker overlay of the objective parameters with annotated comparisons of Compressed SENSE acceleration factor 8 with (CS8-AI) and without (CS8) adaptive intelligence reconstruction to the reference standard Compressed SENSE acceleration factor 4 (CS4). (A) mean apparent signal-to-noise ratio (aSNR) of the three measured regions of interest and (B) corresponding mean apparent contrast-to-noise ratio (aCNR), (C) mean edge rise distance (ERD) of the two vessel edges. ns = not significant; ** = $P < 0.01$; *** = $P < 0.001$.

study on cervical REACT demonstrated significantly improved image quality with CS-AI compared to the clinical standard [27], statistical significance was not achieved in the thoracic aorta despite slightly higher ratings for CS8-AI across all segments. This may be attributable to the greater acceleration increase in the present study (CS4 to CS8 vs CS7 to CS10 in the cervical protocol). Nevertheless, the lack of a significant difference between CS8-AI and CS4 across subjective metrics underscores the clinical equivalence of these protocols. Furthermore, the better performance of CS8-AI relative to CS8 across all segments supports the benefit of deep learning-based denoising, even at high acceleration factors.

Objective measures largely mirrored subjective impressions. As expected, CS8 showed reduced aSNR and aCNR, while CS8-AI restored signal characteristics to levels similar to CS4. Interestingly, the perceived noise in CS8-AI was lower than in CS4, despite comparable aSNR values. This may reflect a focus during subjective rating on intraluminal uniformity, whereas aSNR measurements include background structures such as myocardium. Similarly, perceived edge sharpness in CS8 was lower than in CS4 or CS8-AI, yet ERD measurements showed no significant differences, suggesting that noise perception may have influenced reader judgment of edge sharpness. These findings highlight the limitations of isolated quantitative metrics and support a complementary approach combining objective and reader-based evaluation.

Fat-water swapping artifacts were observed in 17.5 % of subjects being lower than prior reports of thoracic REACT at 3 T (33.3 %[17]) and comparable or even lower than at 1.5 T (16.0 % to 39.7 % [18–20]), which might reflect improved B_0 homogeneity and the absence of metal implants in a healthy volunteer cohort. However, all artifacts were readily identifiable and did not affect interpretability.

Building on the demonstrated diagnostic stability, another major advantage of CS-AI is the substantial reduction in scan duration. While an ideal 50 % time reduction would be expected with 8-fold acceleration, the observed 44 % reduction likely reflects physiologic constraints introduced by ECG triggering and respiratory navigator efficiency. Nonetheless, scan times below five minutes mark a substantial improvement over current non-contrast protocols at 3 T, which typically take 8–10 min [7,8], and increase feasibility for routine clinical use. At 1.5 T, scan durations between six and twelve minutes have been reported [3,5,6,9,19], although the shorter protocols either employed a reduced spatial resolution [19] or limited anatomical coverage in sagittal acquisition [3]. Thus, the results of this study are highly competitive and hold the potential to increase patient comfort, throughput and scheduling flexibility. Reconstruction finishes as the patient leaves, making table turnover rather than imaging the bottleneck.

Future developments may further improve acquisition speed and image quality. In particular, multi-stage convolutional neural networks, such as super-resolution frameworks [34], have demonstrated promising results in 2D protocols (e.g., cine cardiac MRI [35,36]) and might be extended to 3D MRA in the future.

5. Limitations

The selection of a small cohort of healthy volunteers limits the generalizability to clinical populations. Thus, the prevalence of vascular pathology was low, and the diagnostic performance for dissections or postoperative changes remains to be evaluated. Although no evidence of diagnostic inferiority of CS-AI has been reported to date, concerns regarding potential hallucinations or subtle information loss have been raised, and large-scale validation in patient populations is still lacking [37]. Our study focused on aortic diameters, suggesting that diagnostic accuracy can be expected at least for dilatations and stenoses. No comparisons were made with computed tomography angiography (CTA) or contrast-enhanced MRA; however, prior studies have established the diagnostic performance of Dixon-based MRA compared to CTA and contrast-enhanced MRA [3,7,19,20]. Further, the choice of the acceleration factor (CS8/CS8-AI) was guided by prior clinical experience and qualitative pilot scans aimed at achieving comparable image quality to CS4 in substantially shorter scan times while preserving acquired resolution and full thoracic coverage. No formal systematic evaluation of alternative or higher acceleration factors was performed; although further acceleration may be feasible, our pilot scans showed degraded vessel delineation and more artifacts, particularly in peripheral regions. Although readers were blinded to the method, subtle visual differences such as a slightly grainier texture in CS8 compared to the smoother appearance in CS8-AI may have been perceivable. Respiratory motion artifacts had no major impact on image quality, although a narrower dNAV window might increase robustness at the cost of efficiency. Finally, quantitative measures such as aSNR and aCNR are influenced by reconstruction methods and may not reflect absolute noise levels, although trends corresponded well with subjective ratings [38,39]. The provided reconstruction time depends on the hardware and software used and was only recorded in one sample scan. The use of a vendor-specific reconstruction limits generalizability to other systems.

6. Conclusions

In summary, deep learning-based reconstruction enables highly accelerated REACT of the thoracic aorta in less than five minutes with preserved image quality and excellent measurement reproducibility. These findings are likely to expand the use of non-contrast MRA in clinical routine and warrant further studies to evaluate its diagnostic performance in aortic diseases.

CRediT authorship contribution statement

Jan P. Janssen: Writing – original draft, Visualization, Software, Methodology, Investigation, Funding acquisition, Formal analysis, Data curation, Conceptualization. **Roman J. Gertz:** Writing – original draft. **Juliana Tristram:** Writing – review & editing, Validation, Investigation. **Marvin A. Spurek:** Writing – original draft. **Kenan Kaya:** Writing – review & editing, Validation, Investigation. **Robert Terzis:** Writing – review & editing, Validation, Investigation. **Robert Hahnfeldt:** Writing – review & editing, Validation, Investigation. **Thorsten Gietzen:** Writing – review & editing, Resources. **David Maintz:** Writing – review & editing, Supervision, Resources, Conceptualization. **Thorsten Persigehl:** Writing – review & editing, Supervision, Resources, Conceptualization. **Kilian Weiss:** Writing – review & editing, Resources, Methodology. **Lenhard Pennig:** Writing – review & editing, Validation, Supervision, Project administration, Conceptualization. **Carsten Gietzen:** Writing – review & editing, Resources.

Declaration of competing interest

The authors declare that they have no known competing financial interests or personal relationships that could have appeared to influence the work reported in this paper. Roman J. Gertz: Speaker's bureau, Philips Healthcare. Speaker's bureau, Guerbet GmbH. David Maintz: Speaker's bureau, Philips Healthcare. Lenhard Pennig: Speaker's bureau, Philips Healthcare. Speaker's bureau, Guerbet GmbH. Kilian Weiss: Employee, Philips GmbH. The remaining authors disclose no relevant relationships.

Acknowledgments

Supported by the Koeln Fortune Program / Faculty of Medicine, University of Cologne.

Ethics approval and consent to participate/publication.

This prospective single-center study was conducted in accordance with the ethical standards of the 1964 Declaration of Helsinki and its subsequent amendments and was approved by our institutional review board on March 23, 2022 (reference number: 20-1296_1). The study was registered in the German Clinical Trials Register on September 15, 2022 (DRKS00030210). Written informed consent was obtained from all participants.

Appendix A. Supplementary data

Supplementary data to this article can be found online at https://doi.org/10.1016/j.ejrad.2025.112403.

References

[1] M. Czerny, M. Grabenwöger, T. Berger, V. Aboyans, A. Della Corte, E.P. Chen, N.D. Desai, J. Dumfarth, J.A. Elefteriades, C.D. Etz, K.M. Kim, M. Kreibich, M. Lescan, L. Di Marco, A. Martens, C.A. Mestres, M. Milojevic, C.A. Nienaber, G. Piffaretti, O. Preventza, E. Quintana, B. Rylski, C.L. Schlett, F. Schoenhoff, S. Trimarchi, K. Tsagakis, E.S.S.D. Group, EACTS/STS guidelines for diagnosing and treating acute and chronic syndromes of the aortic organ, Eur. J. Cardiothorac. Surg. 65 (2) (2024).

[2] E.M. Isselbacher, O. Preventza, J. Hamilton Black, 3rd, J.G. Augoustides, A.W. Beck, M.A. Bolen, A.C. Braverman, B.E. Bray, M.M. Brown-Zimmerman, E.P. Chen, T.J. Collins, A. DeAnda, Jr., C.L. Fanola, L.N. Girardi, C.W. Hicks, D.S. Hui, W. Schuyler Jones, V. Kalahasti, K.M. Kim, D.M. Milewicz, G.S. Oderich, L. Ogbechie, S.B. Promes, E. Gyang Ross, M.L. Schermerhorn, S. Singleton Times, E.E. Tseng, G. J. Wang, Y.J. Woo, M. Peer Review Committee, 2022 ACC/AHA Guideline for the Diagnosis and Management of Aortic Disease: A Report of the American Heart Association/American College of Cardiology Joint Committee on Clinical Practice Guidelines, Circulation 146(24) (2022) e334-e482.

[3] L. Pennig, A. Wagner, K. Weiss, S. Lennartz, M. Huntgeburth, T. Hickethier, D. Maintz, C.P. Naehle, A.C. Bunck, J. Doerner, Comparison of a novel Compressed SENSE accelerated 3D modified relaxation-enhanced angiography without contrast and triggering with CE-MRA in imaging of the thoracic aorta, Int. J. Cardiovasc. Imaging 37 (1) (2021) 315–329.

[4] S. Veldhoen, C. Behzadi, T. Derlin, M. Rybczinsky, Y. von Kodolitsch, S. Sheikhzadeh, F.O. Henes, T.A. Bley, G. Adam, P. Bannas, Exact monitoring of aortic diameters in Marfan patients without gadolinium contrast: intraindividual comparison of 2D SSFP imaging with 3D CE-MRA and echocardiography, Eur. Radiol. 25 (3) (2015) 872–882.

[5] F. von Knobelsdorff-Brenkenhoff, H. Gruettner, R.F. Trauzeddel, A. Greiser, J. Schulz-Menger, Comparison of native high-resolution 3D and contrast-enhanced MR angiography for assessing the thoracic aorta, European Heart Journal - Cardiovascular Imaging 15 (6) (2014) 651–658.

[6] C.J. François, D. Tuite, V. Deshpande, R. Jerecic, P. Weale, J.C. Carr, Unenhanced MR Angiography of the Thoracic Aorta: initial Clinical Evaluation, Am. J. Roentgenol. 190 (4) (2008) 902–906.

[7] M.G. Zeilinger, D. Giese, M. Schmidt, M.S. May, R. Janka, R. Heiss, F. Ammon, S. Achenbach, M. Uder, C. Treutlein, Highly accelerated, Dixon-based non-contrast MR angiography versus high-pitch CT angiography, Radiol. Med. 129 (2) (2024) 268–279.

[8] F. Wright, M. Warncke, M. Sinn, I. Ristow, A. Lenz, C. Riedel, B.P. Schoennagel, S. Zhang, M.G. Kaul, G. Adam, Y. von Kodolitsch, S. Sehner, P. Bannas, Assessment of aortic diameter in Marfan patients: intraindividual comparison of 3D-Dixon and 2D-SSFP magnetic resonance imaging, Eur. Radiol. 33 (3) (2023) 1687–1697.

[9] A. Fotaki, C. Munoz, Y. Emanuel, A. Hua, F. Bosio, K.P. Kunze, R. Neji, P.G. Masci, R.M. Botnar, C. Prieto, Efficient non-contrast enhanced 3D Cartesian cardiovascular magnetic resonance angiography of the thoracic aorta in 3 min, J. Cardiovasc. Magn. Reson. 24 (1) (2022) 5.

[10] S. Veldhoen, C. Behzadi, A. Lenz, F.O. Henes, M. Rybczynski, Y. von Kodolitsch, T. A. Bley, G. Adam, P. Bannas, Non-contrast MR angiography at 1.5 Tesla for aortic monitoring in Marfan patients after aortic root surgery, J. Cardiovasc. Magn. Reson. 19 (1) (2017) 82.

[11] M. Yoneyama, S. Zhang, H.H. Hu, L.R. Chong, D. Bardo, J.H. Miller, N. Toyonari, K. Katahira, Y. Katsumata, A. Pokorney, C.K. Ng, M. Kouwenhoven, M. Van Cauteren, Free-breathing non-contrast-enhanced flow-independent MR angiography using magnetization-prepared 3D non-balanced dual-echo Dixon method: a feasibility study at 3 Tesla, Magn. Reson. Imaging 63 (2019) 137–146.

[12] E.J. Tan, S. Zhang, P. Tirukonda, L.R. Chong, REACT - a novel flow-independent non-gated non-contrast MR angiography technique using magnetization-prepared 3D non-balanced dual-echo dixon method: Preliminary clinical experience, Eur J Radiol Open 7 (2020) 100238.

[13] J.P. Janssen, S. Rose, K. Kaya, R. Terzis, R. Hahnfeldt, R.J. Gertz, L. Goertz, A. I. Iuga, J.P. Grunz, C. Kabbasch, P. Rauen, T. Persigehl, K. Weiss, J. Borggrefe, L. Pennig, C. Gietzen, Non-contrast-enhanced MR-angiography of Extracranial arteries in Acute Ischemic Stroke at 1.5 Tesla using Relaxation-Enhanced Angiography without Contrast and triggering (REACT), Clin. Neuroradiol. (2024).

[14] L. Pennig, C. Kabbasch, U.C.I. Hoyer, S. Lennartz, D. Zopfs, L. Goertz, K. R. Laukamp, A. Wagner, J.P. Grunz, J. Doerner, T. Persigehl, K. Weiss, J. Borggrefe, Relaxation-Enhanced Angiography without Contrast and triggering (REACT) for Fast Imaging of Extracranial arteries in Acute Ischemic Stroke at 3 T, Clin. Neuroradiol. 31 (3) (2021) 815–826.

[15] C. Gietzen, K. Kaya, J.P. Janssen, R.J. Gertz, R. Terzis, H. Huflage, J.P. Grunz, T. Gietzen, H. Pennig, E. Celik, J. Borggrefe, T. Persigehl, C. Kabbasch, K. Weiss, L. Goertz, L. Pennig, Highly compressed SENSE accelerated relaxation-enhanced angiography without contrast and triggering (REACT) for fast non-contrast enhanced magnetic resonance angiography of the neck: Clinical evaluation in patients with acute ischemic stroke at 3 tesla, Magn. Reson. Imaging 112 (2024) 27–37.

[16] L. Pennig, A. Wagner, K. Weiss, S. Lennartz, J.P. Grunz, D. Maintz, K.R. Laukamp, T. Hickethier, C.P. Naehle, A.C. Bunck, J. Doerner, Imaging of the pulmonary vasculature in congenital heart disease without gadolinium contrast: Intraindividual comparison of a novel Compressed SENSE accelerated 3D modified REACT with 4D contrast-enhanced magnetic resonance angiography, J. Cardiovasc. Magn. Reson. 22 (1) (2020) 8.

[17] A. Isaak, N. Mesropyan, C. Hart, S. Zhang, D. Kravchenko, C. Endler, C. Katemann, O. Weber, C.C. Pieper, D. Kuetting, U. Attenberger, D. Dabir, J.A. Luetkens, Non-contrast free-breathing 3D cardiovascular magnetic resonance angiography using REACT (relaxation-enhanced angiography without contrast) compared to contrast-enhanced steady-state magnetic resonance angiography in complex pediatric congenital heart disease at 3T, J. Cardiovasc. Magn. Reson. 24 (1) (2022) 55.

[18] A. Isaak, J.A. Luetkens, A. Faron, C. Endler, N. Mesropyan, C. Katemann, S. Zhang, P. Kupczyk, D. Kuetting, U. Attenberger, D. Dabir, Free-breathing non-contrast flow-independent cardiovascular magnetic resonance angiography using cardiac gated, magnetization-prepared 3D Dixon method: assessment of thoracic vasculature in congenital heart disease, J. Cardiovasc. Magn. Reson. 23 (1) (2021) 91.

[19] C. Gietzen, J.P. Janssen, J. Tristram, B. Cagman, K. Kaya, R. Terzis, R. Gertz, T. Gietzen, H. Pennig, A.C. Bunck, D. Maintz, T. Persigehl, N. Mader, K. Weiss, L. Pennig, Assessment of the thoracic aorta after aortic root replacement and/or ascending aortic surgery using 3D relaxation-enhanced angiography without contrast and triggering, Front. Cardiovasc. Med. 12–2025 (2025).

[20] C. Gietzen, L. Pennig, J. von Stein, H. Guthoff, K. Weiss, R. Gertz, I. Thurbach, A. C. Bunck, D. Maintz, S. Baldus, H. Ten Freyhaus, C. Hohmann, P. von Stein, Thoracic aorta diameters in Marfan patients: Intraindividual comparison of 3D modified relaxation-enhanced angiography without contrast and triggering (REACT) with transthoracic echocardiography, Int. J. Cardiol. 390 (2023) 131203.

[21] G. Bratke, R. Rau, K. Weiss, C. Kabbasch, K. Sircar, J.N. Morelli, T. Persigehl, D. Maintz, D. Giese, S. Haneder, Accelerated MRI of the Lumbar Spine using Compressed Sensing: Quality and Efficiency, J. Magn. Reson. Imaging 49 (7) (2019) e164–e175.

[22] M. Lustig, D. Donoho, J.M. Pauly, Sparse MRI: the application of compressed sensing for rapid MR imaging, Magn. Reson. Med. 58 (6) (2007) 1182–1195.

[23] N. Pezzotti, S. Yousefi, M.S. Elmahdy, J.H.F.V. Gemert, C. Schuelke, M. Doneva, T. Nielsen, S. Kastryulin, B.P.F. Lelieveldt, M.J.P.V. Osch, E.D. Weerdt, M. Staring, An Adaptive Intelligence Algorithm for Undersampled knee MRI Reconstruction, IEEE Access 8 (2020) 204825–204838.

[24] N. Pezzotti, E. de Weerdt, S. Yousefi, M.S. Elmahdy, J. van Gemert, C. Schülke, M. Doneva, T. Nielsen, S. Kastryulin, B.P. Lelieveldt, Adaptive-CS-Net: FastMRI with adaptive intelligence, arXiv preprint arXiv:1912.12259 (2019).

[25] A. Pednekar, M. Kocaoglu, H. Wang, A. Tanimoto, J.A. Tkach, S. Lang, M.D. Taylor, Accelerated Cine Cardiac MRI using Deep Learning-based Reconstruction: a Systematic Evaluation, J. Magn. Reson. Imaging 60 (2) (2024) 640–650.

[26] X. Wu, L. Deng, W. Li, P. Peng, X. Yue, L. Tang, Q. Pu, Y. Ming, X. Zhang, X. Huang, Y. Chen, J. Huang, J. Sun, Deep Learning-based Acceleration of Compressed Sensing for Noncontrast-Enhanced Coronary magnetic Resonance Angiography in patients with Suspected Coronary Artery Disease, J. Magn. Reson. Imaging 58 (5) (2023) 1521–1530.

[27] J.P. Janssen, K. Kaya, R. Terzis, R. Hahnfeldt, R.J. Gertz, L. Goertz, S. Skornitzke, J. Tristram, T. Dratsch, C. Goezdas, C. Kabbasch, K. Weiss, L. Pennig, C.H. Gietzen, Sub-1-min relaxation-enhanced non-contrast non-triggered cervical MRA using compressed SENSE with deep learning reconstruction in healthy volunteers, Eur. Radio. Exp. 9 (1) (2025) 19.

[28] D. Liang, B. Liu, J. Wang, L. Ying, Accelerating SENSE using compressed sensing, Magn. Reson. Med. 62 (6) (2009) 1574–1584.

[29] J.M. Weinrich, M. Avanesov, A. Lenz, E. Tahir, F.O. Henes, B.P. Schoennagel, M. Rybczinsky, G. Adam, Y. von Kodolitsch, P. Bannas, Reliability of non-contrast magnetic resonance angiography-derived aortic diameters in Marfan patients: comparison of inner vs. outer vessel wall measurements, Int. J. Cardiovasc. Imaging 36 (8) (2020) 1533–1542.

[30] N. Kawel-Boehm, A. Maceira, E.R. Valsangiacomo-Buechel, J. Vogel-Claussen, E. B. Turkbey, R. Williams, S. Plein, M. Tee, J. Eng, D.A. Bluemke, Normal values for cardiovascular magnetic resonance in adults and children, J. Cardiovasc. Magn. Reson. 17 (1) (2015) 29.

[31] U.C.I. Hoyer, S. Lennartz, N. Abdullayev, F. Fichter, S.T. Junger, L. Goertz, K. R. Laukamp, R.J. Gertz, J.P. Grunz, C. Hohmann, D. Maintz, T. Persigehl, C. Kabbasch, J. Borggrefe, K. Weiss, L. Pennig, Imaging of the extracranial internal carotid artery in acute ischemic stroke: assessment of stenosis, plaques, and image quality using relaxation-enhanced angiography without contrast and triggering (REACT), Quant. Imaging Med. Surg. 12 (7) (2022) 3640–3654.

[32] J.A. Elefteriades, S.K. Mukherjee, H. Mojibian, Discrepancies in Measurement of the Thoracic Aorta: JACC Review Topic of the Week, J. Am. Coll. Cardiol. 76 (2) (2020) 201–217.

[33] A. Lenz, M. Warncke, F. Wright, J.M. Weinrich, B.P. Schoennagel, F.O. Henes, G. Adam, Y. von Kodolitsch, G. Schoen, P. Bannas, Longitudinal follow-up by MR angiography reveals progressive dilatation of the distal aorta after aortic root replacement in Marfan syndrome, Eur. Radiol. 33 (10) (2023) 6984–6992.

[34] C. Dong, C.C. Loy, K. He, X. Tang, Image Super-Resolution using Deep Convolutional Networks, IEEE Trans. Pattern Anal. Mach. Intell. 38 (2) (2016) 295–307.

[35] T. Aziz-Safaie, L.M. Bischoff, C. Katemann, J.M. Peeters, D. Kravchenko, N. Mesropyan, L.D. Beissel, T. Dell, O.M. Weber, C.C. Pieper, D. Kütting, J.A. Luetkens, A. Isaak, Fast and Robust Single-Shot Cine Cardiac MRI Using Deep Learning Super-Resolution Reconstruction, Investigative Radiology (9900) 10.1097/RLI.0000000000001186.

[36] D. Kravchenko, A. Isaak, N. Mesropyan, J.M. Peeters, D. Kuetting, C.C. Pieper, C. Katemann, U. Attenberger, T. Emrich, A. Varga-Szemes, J.A. Luetkens, Deep learning super-resolution reconstruction for fast and high-quality cine cardiovascular magnetic resonance, Eur. Radiol. 35 (5) (2025) 2877–2887.

[37] S.J. Fransen, C. Roest, F.F.J. Simonis, D. Yakar, T.C. Kwee, The scientific evidence of commercial AI products for MRI acceleration: a systematic review, Eur. Radiol. 35 (8) (2025) 4736–4746.

[38] O. Dietrich, J.G. Raya, S.B. Reeder, M.F. Reiser, S.O. Schoenberg, Measurement of signal-to-noise ratios in MR images: influence of multichannel coils, parallel imaging, and reconstruction filters, J. Magn. Reson. Imaging 26 (2) (2007) 375–385.

[39] O. Dietrich, J.G. Raya, S.B. Reeder, M. Ingrisch, M.F. Reiser, S.O. Schoenberg, Influence of multichannel combination, parallel imaging and other reconstruction techniques on MRI noise characteristics, Magn. Reson. Imaging 26 (6) (2008) 754–762.